Deregulation of MMR-Related Pathways and Anticancer Potential of Curcuma Derivatives– A Computational Approach

Priyanjali Bhattacharya[1], Trupti N Patel[1*]

[1]Department of Integrative Biology, Vellore Institute of Technology, Vellore, India

[*]Corresponding Address- tnpatel@vit.ac.in, Dr.TNPatel@gmail.com

Supplementary Data

Distribution of Mutations among the Genes (selected) involved in Hematologic Malignancies from COSMIC Database and a brief mutational profile using various *in silico* tools

Abbreviations -
*nsSNPs obtained from COSMIC; grey highlights- substitutions that are highly damaging considering ≥3 out of 5 different algorithms; N- Neutral, D- damaging, B-benign, NA- not applicable

- Link 1- ABL1; https://cancer.sanger.ac.uk/cosmic/gene/analysis?all_data=&coords=AA%3AAA&dr=&end=1150&gd=&id=368134&ln=ABL1&seqlen=1150&sn=haematopoietic_and_lymphoid_tissue&start=1#ts

Table S1: *In silico* analysis of missense substitutions of abl1 protein

Mutation	Polyphen2.0	Panther	PhD-SNP	SIFT	SNAP
G6R	0.999 D	NA	0.398 N	0.180 N	0.430 N
A53P	0.009 B	NA	0.475 N	0.130 N	0.380 N
A75T	0.041 B	NA	0.563 D	0.060 N	0.295 N
Y272H	1.000 D	0.548 D	0.537 D	0.000 D	0.820 D
D344N	0.900 D	0.270 N	0.446 N	0.060 N	0.210 N
N689S	0.537 D	NA	0.337 N	0.890 N	0.245 N
V806M	0.483 D	NA	0.389 N	0.010 D	0.565 D
T1084S	0.649 D	NA	0.680 D	0.000 D	0.560 D
K1099T	0.997 D	NA	0.801 D	0.010 D	0.720 D
C1119F	0.999 D	NA	0.878 D	0.220 N	0.655 D
E187K	0.288 B	0.251 N	0.194 N	0.090 N	0.375 N
D295G	0.243 B	0.520 D	0.204 N	0.040 D	0.460 N
E301V	0.991 D	0.530 D	0.675 D	0.000 D	0.600 D
T334I	0.999 D	0.496 N	0.736 D	0.020 D	0.470 N
T334L	1.000 D	0.463 N	0.713 D	0.030 D	0.765 D
A621T	0.280 B	NA	0.421 N	0.300 N	0.200 N
P937L	0.018 B	NA	0.270 N	0.000 D	0.675 D
A1010T	0.000 B	NA	0.093 N	0.000 D	0.605 D
G60D	0.016 B	NA	0.575 D	0.870 N	0.285 N
G269E	0.975 D	0.606 D	0.332 N	0.150 N	0.425 N
F330I	0.915 D	0.462 N	0.116 N	0.290 N	0.165 N
F336R	1.000 D	0.637 D	0.852 D	0.000 D	0.765 D
F336L	0.942 D	0.292 N	0.373 N	0.280 N	0.445 N
M370T	1.000 D	0.953 D	0.905 D	0.000 D	0.705 D
E374G	1.000 D	0.529 D	0.781 D	0.000 D	0.630 D
F378I	0.992 D	0.501 D	0.776 D	0.040 D	0.515 D
L389R	1.000 D	0.991 D	0.923 D	0.000 D	0.715 D
H415R	0.002 B	0.544 D	0.316 N	0.130 N	0.300 N

- Link 2- MYC gene; https://cancer.sanger.ac.uk/cosmic/gene/analysis?all_data=&coords=AA%3AAA&dr=&end=455&gd=&id=359910&ln=MYC&seqlen=455&sn=haematopoietic_and_lymphoid_tissue&start=1#ts

Table S2: *In silico* analysis of missense substitutions of myc protein

Mutation	Polyphen2.0	Panther	PhD-SNP	SIFT	SNAP
Q11R	0.167 B	NA	0.621 D	NA	0.435 N
S21N	0.001 B	0.154 N	0.315 N	NA	0.390 N
A59V	1.000 D	0.593 D	0.193 N	NA	0.450 N
P72L	0.999 D	0.982 D	0.559 D	NA	0.590 D
T73A	0.663 D	0.766 D	0.341 N	NA	0.415 N
T73I	0.981 D	0.919 D	0.483 N	NA	0.565 D
T73N	0.999 D	0.913 D	0.531 D	NA	0.425 N
P74A	1.000 D	0.916 D	0.289 N	NA	0.620 D
P74L	1.000 D	0.960 D	0.446 N	NA	0.590 D
P74Q	1.000 D	0.971 D	0.546 D	NA	0.625 D
P74R	1.000 D	0.961 D	0.433 N	NA	0.660 D
P74S	1.000 D	0.930 D	0.383 N	NA	0.625 D
P75S	0.999 D	0.450 N	0.320 N	NA	0.585 D
L97V	0.058 D	0.047 N	0.372 N	NA	0.280 N
R98Q	0.856 D	0.067 N	0.347 N	NA	0.440 N
N127K	0.170 B	0.168 N	0.516 D	0.020 D	0.500 N
F130L	0.562 D	0.208 N	0.507 D	0.160 N	0.445 N
F153S	0.991 D	0.935 D	0.849 D	0.030 D	0.660 D
A156S	0.481 D	0.221 N	0.279 N	0.220 N	0.130 N
S161L	0.840 D	0.367 N	0.555 D	0.030 D	0.490 N
V6G	0.000 B	NA	0.448 N	NA	0.550 D
Y47C	0.999 D	0.862 D	0.481 N	NA	0.665 D
Q52R	0.372 B	0.432 N	0.074 N	NA	0.475 N
S53T	0.955 D	0.298 N	0.083 N	NA	0.425 N
E54D	0.056 B	0.187 N	0.074 N	NA	0.490 N
A59V	1.000 D	0.593 D	0.193 N	NA	0.450 N
L71V	0.999 D	0.782 D	0.110 N	NA	0.520 D
P72S	0.778 D	0.969 D	0.451 N	NA	0.630 D
P72T	0.995 D	0.976 D	0.450 N	NA	0.635 D
Y89H	0.965 D	0.254 N	0.260 N	NA	0.415 N
D102G	0.000 B	0.199 N	0.359 N	NA	0.605 D
I144L	0.486 D	0.258 N	0.617 D	0.310 N	0.375 N
F153C	0.998 D	0.971 D	0.827 D	0.010 D	0.705 D
S189V	0.045 D	0.364 N	0.182 N	0.210 N	0.345 N
L191M	0.988 D	0.369 N	0.114 N	0.080 N	0.330 N

- Link 3- MAX gene; https://cancer.sanger.ac.uk/cosmic/gene/analysis?all_data=&coords=AA%3AAA&dr=&end=161&gd=&id=209776&ln=MAX&seqlen=161&sn=haematopoietic_and_lymphoid_tissue&start=1#distribution

Table S3: *In silico* analysis of missense substitutions of max protein

Mutation	Polyphen2.0	Panther	PhD-SNP	SIFT	SNAP
R35H	1.000 D	0.816 D	0.672 D	NA	NA
R36W	1.000 D	0.941 D	0.715 D	NA	NA
D37G	1.000 D	0.708 D	0.661 D	NA	NA
N120T	0.000 B	0.067 N	0.170 N	NA	NA
R60Q	1.000 D	0.661 D	0.404 N	NA	NA

- Link 4- MYB gene; https://cancer.sanger.ac.uk/cosmic/gene/analysis?all_data=&coords=AA%3AAA&dr=&end=762&gd=&id=303929&ln=MYB&seqlen=762&sn=haematopoietic_and_lymphoid_tissue&start=1#distribution

Table S4: *In silico* analysis of missense substitutions of myb protein

Mutation	Polyphen2.0	Panther	PhD-SNP	SIFT	SNAP
E14K	0.900 D	NA	0.590 D	0.020 D	0.660 D
E14Q	0.967 D	NA	0.308 N	0.020 D	0.585 D
K35N	0.996 D	NA	0.550 D	0.010 D	0.650 D
N68I	0.055 B	NA	0.268 N	0.070 N	0.565 D
N68Y	0.864 D	NA	0.283 N	0.040 D	0.665 D
W82R	1.000 D	0.939 D	0.864 D	0.260 N	0.865 D
S146P	0.170 B	0.703 D	0.224 N	0.160 N	0.470 N
E299K	1.000 D	0.305 N	0.806 D	0.020 D	0.575 D
L301F	1.000 D	0.269 N	0.564 D	0.040 D	0.500 N
T427I	0.096 B	NA	0.210 N	0.250 N	0.325 N
C322Y	0.210 B	0.267 N	0.566 D	0.030 D	0.690 D
S745T	0.015 B	NA	0.366 N	0.250 N	0.270 N
F661Y	0.997 D	NA	0.470 N	0.000 D	0.555 D
R510S	0.017 B	NA	0.057 N	0.430 N	0.450 N
D408G	0.995 D	NA	0.651 D	0.390 N	0.470 N
W82R	0.997 D	0.939 D	0.864 D	0.000 D	0.900 D
T427I	0.096 B	NA	0.204 N	0.020 D	0.520 D
K387N	0.791 D	0.212 N	0.594 D	0.390 N	0.345 N

- Link 5- PCNA gene; https://cancer.sanger.ac.uk/cosmic/gene/analysis?all_data=&coords=AA%3AAA&dr=&end=262&gd=&id=343943&ln=PCNA&seqlen=262&sn=haematopoietic_and_lymphoid_tissue&start=1#ts

Table S5: *In silico* analysis of missense substitutions of pcna protein

Mutation	Polyphen2.0	Panther	PhD-SNP	SIFT	SNAP
R61H	0.971 D	0.504 D	0.712 D	0.030 D	0.680 D

- Link 6- TOP3A gene; https://cancer.sanger.ac.uk/cosmic/gene/analysis?all_data=&coords=AA%3AAA&dr=&end=1002&gd=&id=280375&ln=TOP3A&seqlen=1002&sn=haematopoietic_and_lymphoid_tissue&start=1#distribution

Table S6: *In silico* analysis of missense substitutions of top3a protein

Mutation	Polyphen2.0	Panther	PhD-SNP	SIFT	SNAP
E398K	0.302 B	0.527 D	0.385 N	0.390 N	0.290 N
A461T	0.995 D	0.745 D	0.339 N	0.050 D	0.515 D
T504N	0.026 D	0.600 D	0.109 N	0.500 N	0.095 N
P514T	1.000 D	0.855 D	0.702 D	0.000 D	0.645 D
I647T	0.008 B	0.317 N	0.242 N	0.620 N	0.290 N
R722C	0.990 D	0.904 D	0.733 D	0.150 N	0.620 D
V811M	0.967 D	0.614 D	0.532 D	0.060 N	0.530 D
P990S	0.959 D	NA	0.271 N	0.040 D	0.615 D

- Link 7- P73 gene; https://cancer.sanger.ac.uk/cosmic/gene/analysis?all_data=&coords=AA%3AAA&dr=&end=637&gd=&id=386532&ln=TP73&seqlen=637&sn=haematopoietic_and_lymphoid_tissue&start=1#distribution

Table S7: *In silico* analysis of missense substitutions of p73 protein

Mutation	Polyphen2.0	Panther	PhD-SNP	SIFT	SNAP
H17L	0.998 D	NA	0.254 N	0.030 D	0.500 N
P111L	1.000 D	NA	0.398 N	0.110 N	0.445 N
S145C	1.000 D	0.959 D	0.663 D	0.000 D	0.745 D
V191M	1.000 D	0.897 D	0.727 D	0.000 D	0.640 D
P195L	0.780 D	0.963 D	0.771 D	0.040 D	0.605 D
E205K	0.607 D	0.421 N	0.440 N	0.050 N	0.515 D
G219D	0.993 D	0.954 D	0.845 D	0.080 N	0.545 D
Y487D	1.000 D	0.684 D	0.687 D	0.060 N	0.655 D
I626V	0.995 D	NA	0.376 N	0.230 N	0.530 D

- Link 8- BLM gene; https://cancer.sanger.ac.uk/cosmic/gene/analysis?all_data=&coords=AA%3AAA&dr=&end=1418&gd=&id=399159&ln=BLM&seqlen=1418&sn=haematopoietic_and_lymphoid_tissue&start=1#ts

Table S8: *In silico* analysis of missense substitutions of blm protein

Mutation	Polyphen2.0	Panther	PhD-SNP	SIFT	SNAP
F32I	0.046 B	NA	0.333 N	0.060 N	0.470 N
R85T	0.002 B	NA	0.248 N	0.000 D	0.640 D
M348I	0.146 B	NA	0.341 N	0.060 N	0.535 D
G397W	1.000 D	NA	0.867 D	0.000 D	0.705 D
S601Y	0.947 D	NA	0.354 N	0.020 D	0.550 D
R643H	0.004 B	0.325 N	0.378 N	0.520 N	0.240 N
S646G	0.000 B	0.081 N	0.095 N	1.000 N	0.125 N
Q672R	1.000 D	0.995 D	0.885 D	0.000 D	0.870 D
R791C	0.981 D	0.885 D	0.795 D	0.010 D	0.595 D
H805Y	1.000 D	0.864 D	0.853 D	0.000 D	0.745 D
L879V	0.063 B	0.082 N	0.306 N	0.280 N	0.185 N
H886N	0.048 B	0.357 N	0.446 N	0.040 D	0.455 N
D906N	0.018 B	0.183 N	0.192 N	0.120 N	0.080 N
Q909R	0.013 B	0.145 N	0.212 N	0.260 N	0.260 N
P956L	0.992 D	0.779 D	0.862 D	0.000 D	0.490 N
Y1044C	1.000 D	0.841 D	0.924 D	0.000 D	0.745 D
D1076H	1.000 D	0.552 D	0.691 D	0.000 D	0.755 D
V1077M	0.890 D	0.567 D	0.205 N	0.090 N	0.240 N
D1080N	0.699 D	0.276 N	0.267 N	0.090 N	0.180 N
V1198M	0.017 B	0.232 N	0.195 N	0.020 D	0.270 N
V1321I	0.010 B	NA	0.084 N	0.230 N	0.370 N
V1321L	0.092 B	NA	0.443 N	0.200 N	0.495 N
S1368Y	0.906 D	NA	0.569 D	0.030 D	0.580 D

Model and Structure Validation of myb protein using Phyre2 and PROCHECK Ramachandran Plot

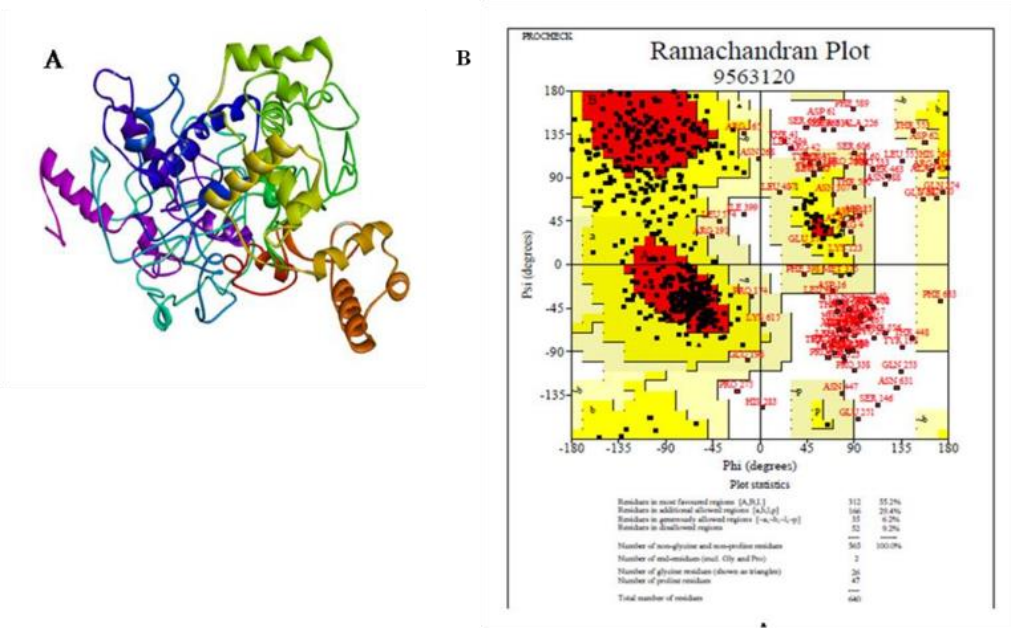

Figure 1: (A) 3D model of myb protein (B) Ramachandran plot of myb protein

Table S9: PROCHECK Ramachandran plot analysis result of myb protein

Protein	No. of residues in most favoured regions	No. of residues in additional allowed regions	No. of residues in generously allowed regions	No. of residues in disallowed regions
myb	55.2%	29.4%	6.2%	9.2%

Active Binding Site and Residues involved in the target proteins using MetaPocket2.0

Table S10: Active binding site residues of abl1

BINDING POCKET 1	ALA_A^93^ SER_A^94^ TYR_A^283^ LEU_A^285^ VAL_A^92^ LYS_A^282^ SER_A^284^ VAL_A^247^ PHE_A^91^ TRP_A^280^ LEU_A^321^ GLY_A^246^ VAL_A^244^ SER_A^248^ VAL_A^287^ GLU_A^335^ TYR_A^245^ THR_A^286^ PHE_A^336^ GLN_A^319^ LYS_A^241^ TYR_A^134^ THR_A^243^ PRO_A^242^ ASP_A^90^ MET_A^337^ THR_A^338^ LYS_A^397^ LEU_A^320^ ASN_A^240^ GLU_A^392^ LEU_A^395^ ASN_A^133^ PRO_A^315^ GLY_A^391^ HIS_A^314^ LEU_A^88^ TYR_A^89^ SER_A^132^ ILE_A^135^ TYR_A^339^ THR_A^136^ ASN_A^393^ GLU_A^142^ ASN_A^316^ ARG_A^239^ LYS_A^313^ SER_A^368^ TYR_A^372^ LYS_A^375^ GLU_A^371^ LYS_A^238^ PRO_A^150^ TYR_A^147^ GLN_A^365^ GLU_A^174^ HIS_A^148^ GLY_A^149^ HIS_A^394^ TYR_A^361^ VAL_A^396^ HIS_A^144^ VAL_A^151^ HIS_A^509^ TYR_A^158^ LEU_A^159^ THR_A^364^ PRO_A^237^ ALA_A^155^ GLU_A^513^ SER_A^152^ SER_A^175^ GLU_A^172^ GLN_A^510^ SER_A^173^ ASN_A^154^ ARG_A^153^ VAL_A^357^ LEU_A^360^ ARG_A^171^ GLN_A^179^ THR_A^514^ SER_A^176^ SER_A^181^ ARG_A^180^ GLN_A^517^ ARG_A^194^ HIS_A^192^ PHE_A^516^ TYR_A^193^ GLU_A^518^ LYS_A^376^
BINDING POCKET 2	HIS_A^314^ PRO_A^315^ ASN_A^316^ SER_A^368^ PRO_A^150^ GLU_A^174^ ARG_A^239^ VAL_A^151^ SER_A^152^ ALA_A^155^ GLU_A^513^ SER_A^175^ GLN_A^510^ ARG_A^153^ SER_A^173^ ARG_A^171^ GLU_A^172^ GLN_A^517^ THR_A^514^ TYR_A^158^ LEU_A^159^ ASN_A^393^ LYS_A^238^ PRO_A^237^ SER_A^162^ TYR_A^361^ TYR_A^89^ HIS_A^148^ ASN_A^240^ TYR_A^147^ GLY_A^149^ SER_A^161^ HIS_A^394^ GLN_A^352^ GLU_A^353^ ASN_A^355^ VAL_A^358^ ASN_A^154^ GLU_A^157^ HIS_A^192^ PHE_A^516^ SER_A^519^ SER_A^520^ ILE_A^521^ VAL_A^357^ LEU_A^360^ THR_A^364^ GLN_A^365^ HIS_A^509^
BINDING POCKET 3	ALA_A^452^ THR_A^453^ MET_A^456^ PRO_A^480^ GLU_A^481^ TRP_A^449^ GLU_A^478^ ARG_A^479^ ARG_A^351^ TYR_A^454^ TYR_A^459^ PRO_A^460^ TYR_A^475^ MET_A^477^ ILE_A^462^ ASN_A^355^ ALA_A^356^ VAL_A^525^ GLY_A^482^ LEU_A^529^ CYS_A^483^ PRO_A^484^ VAL_A^487^ ILE_A^521^ LEU_A^359^ ILE_A^451^ LEU_A^360^ LEU_A^448^ ALA_A^363^ PHE_A^512^
BINDING POCKET 4	GLU_A^274^ THR_A^291^ LEU_A^292^ LYS_A^293^ GLU_A^298^ PHE_A^302^ GLY_A^273^ LYS_A^290^ TYR_A^272^ GLU_A^305^ GLU_A^301^ PHE_A^401^ GLY_A^402^ ARG_A^381^ LEU_A^403^ LYS_A^304^ SER_A^404^ VAL_A^308^ ASP_A^400^ ARG_A^405^ PHE_A^378^ THR_A^296^ GLU_A^300^ LEU_A^303^ VAL_A^275^ HIS_A^415^ TYR_A^412^ ALA_A^418^ GLN_A^271^ ALA_A^414^ ASN_A^382^ THR_A^413^ GLY_A^270^ ALA_A^416^ HIS_A^380^ LYS_A^419^ PHE_A^420^ ASN_A^387^ PHE_A^435^ PRO_A^421^ ARG_A^386^ THR_A^425^ LEU_A^383^ ALA_A^384^ ILE_A^422^ ASP_A^440^ SER_A^439^ TRP_A^424^ ALA_A^443^ ALA_A^426^ LYS_A^423^ TRP_A^442^
BINDING POCKET 5	LYS_A^238^ ARG_A^239^ ASN_A^393^ PRO_A^237^ ASN_A^240^ TYR_A^158^ LEU_A^159^ HIS_A^394^ TYR_A^361^ ALA_A^236^ SER_A^162^ GLU_A^353^ SER_A^161^ VAL_A^358^ GLY_A^163^ TYR_A^234^ SER_A^167^ LEU_A^160^ VAL_A^354^ GLU_A^157^ GLN_A^352^ ASN_A^355^ LEU_A^359^ LEU_A^360^ ALA_A^363^ LEU_A^448^ ILE_A^451^ ALA_A^452^ PHE_A^512^ VAL_A^487^ ILE_A^521^ THR_A^364^ ALA_A^356^ VAL_A^357^ CYS_A^483^ ARG_A^185^ VAL_A^190^ ARG_A^351^ THR_A^453^ TYR_A^454^ MET_A^456^ PRO_A^484^ VAL_A^525^ SER_A^522^ GLY_A^188^ TYR_A^459^ PRO_A^460^ ILE_A^462^ TYR_A^475^ MET_A^477^ TRP_A^449^ GLU_A^478^ PRO_A^480^ GLU_A^481^ SER_A^520^ ARG_A^189^ GLY_A^461^ ARG_A^476^ ARG_A^479^ GLY_A^482^ HIS_A^192^ LEU_A^529^ ASP_A^523^ TYR_A^191^ ARG_A^153^ SER_A^519^ GLU_A^518^ PHE_A^516^ GLN_A^517^ GLU_A^526^ GLU_A^187^

Table S11: Active binding site residues of myc

BINDING POCKET 1	PHE_C^921^ PHE_C^922^ ALA_C^937^ LYS_C^939^ ILE_C^942^ ARG_C^914^ LEU_C^917^ LYS_C^918^ GLU_C^935^ PRO_C^938^ ARG_C^925^ ASN_C^934^ LYS_C^936^
BINDING POCKET 2	LEU_C^924^ GLN_C^927^ ILE_C^928^ ALA_C^946^ TYR_C^949^ ILE_C^950^ VAL_C^953^ GLN_C^954^ GLU_C^957^ GLU_C^956^ LEU_C^960^ LYS_C^945^ THR_C^947^ PRO_C^929^ ASP_C^926^ ALA_C^948^
BINDING POCKET 3	ARG_C^968^ LYS_C^969^ ARG_C^971^ GLU_C^972^
BINDING POCKET 4	ILE_C^928^ GLU_C^930^ LYS_C^945^ ALA_C^948^ TYR_C^949^ PRO_C^929^ SER_C^952^ ALA_C^946^ LYS_C^944^
BINDING POCKET 5	ARG_C^971^ LEU_C^974^ LYS_C^975^

Table S12: Active binding site residues of max

BINDING POCKET 1	LYS_9^89^ ASN_9^92^ ALA_9^93^ GLU_9^96^ GLN_9^112^ ASN_9^114^ LEU_9^111^ ARG_9^100^ THR_9^113^ SER_9^140^ GLY_9^137^ GLY_9^136^ THR_9^130^ LEU_9^122^ PRO_9^116^ ALA_9^133^ SER_9^138^ GLU_9^103^ SER_9^141^ VAL_9^99^ ILE_9^131^ SER_9^142^ PHE_9^134^ ASP_9^135^ SER_9^121^ SER_9^129^ ALA_9^126^ TYR_9^123^ THR_9^124^ SER_9^117^ SER_9^108^ ALA_9^109^ ALA_9^101^ LEU_9^102^ LYS_9^104^ SER_9^107^ GLN_9^98^ ARG_9^106^ LEU_9^95^ ALA_9^105^ GLN_9^110^ SER_9^118^ ASN_9^125^ SER_9^144^ GLU_9^145^
BINDING POCKET 2	SER_9^2^ ASP_9^12^ GLN_9^19^ ASP_9^23^ ALA_9^26^ HIS_9^27^ ALA_9^30^ MET_9^1^ ASP_9^3^ ASN_9^4^ ASP_9^5^ GLU_9^10^ GLN_9^15^ PRO_9^16^ SER_9^11^ GLU_9^8^ GLU_9^13^ ASP_9^6^ VAL_9^9^ ILE_9^7^
BINDING POCKET 3	LYS_9^57^ ALA_9^58^ SER_9^59^ ARG_9^60^ LYS_9^40^ ILE_9^63^ PHE_9^43^ ARG_9^47^ HIS_9^44^
BINDING POCKET 4	LEU_9^122^ ASN_9^125^ ALA_9^126^ ALA_9^133^ PHE_9^134^ ASP_9^135^ GLY_9^136^ LYS_9^127^ SER_9^132^ SER_9^117^ SER_9^140^ SER_9^141^ SER_9^142^ GLU_9^145^ GLU_9^147^ TYR_9^123^ THR_9^124^ SER_9^144^ ASN_9^120^ SER_9^121^
BINDING POCKET 5	ARG_9^152^ LYS_9^154^ SER_9^151^ LYS_9^153^ ARG_9^156^ PRO_9^149^ GLN_9^150^ GLU_9^158^ GLU_9^147^ GLU_9^148^ ALA_9^159^ ASP_9^119^ MET_9^157^ SER_9^160^ ASN_9^120^ GLU_9^145^ PRO_9^146^ SER_9^117^ SER_9^118^ SER_9^144^ GLN_9^110^ TYR_9^115^ LEU_9^122^ SER_9^121^ SER_9^142^

Table S13: Active binding site residues of myb

BINDING POCKET 1	GLU_9^292^ LEU_9^569^ THR_9^570^ ILE_9^295^ LEU_9^300^ PRO_9^358^ PHE_9^589^ LYS_9^587^ ASN_9^567^ LEU_9^301^ LEU_9^302^ GLU_9^297^ SER_9^571^ ALA_9^276^ LEU_9^357^ LEU_9^586^ ILE_9^568^ PRO_9^275^ LEU_9^298^ LYS_9^296^ PRO_9^566^ GLN_9^274^ ALA_9^565^ MET_9^303^ ALA_9^278^ ALA_9^588^ PRO_9^355^ GLU_9^582^ ASP_9^583^ GLN_9^281^ ALA_9^279^ ILE_9^280^ ARG_9^294^ THR_9^354^ ALA_9^359^ ASP_9^360^ SER_9^579^ ILE_9^269^ VAL_9^270^ ARG_9^282^ THR_9^590^ HIS_9^352^ SER_9^353^ MET_9^575^ PRO_9^577^ ASP_9^27^ ASN_9^271^ GLU_9^580^ ALA_9^576^ ASP_9^564^ VAL_9^267^ GLY_9^28^ LEU_9^487^ ALA_9^264^ MET_9^21^ HIS_9^351^ TYR_9^26^ LEU_9^29^ MET_9^486^ VAL_9^263^ SER_9^257^ PRO_9^31^ SER_9^256^ HIS_9^258^ ASN_9^268^ GLN_9^489^ GLY_9^362^ LEU_9^30^ ALA_9^563^ THR_9^490^ MET_9^221^ LYS_9^192^ LEU_9^364^ PRO_9^491^ VAL_9^193^ SER_9^363^ PRO_9^361^ ASN_9^285^ ASP_9^286^ LYS_9^293^ HIS_9^283^ LYS_9^291^ SER_9^572^ LEU_9^574^ GLU_9^299^ ALA_9^277^ ASN_9^584^ SER_9^356^ PRO_9^365^ SER_9^368^ PRO_9^561^ GLU_9^547^ VAL_9^562^ SER_9^304^ PRO_9^273^ ALA_9^578^ PRO_9^488^ ASP_9^18^ GLU_9^194^ LEU_9^348^ GLU_9^196^ GLN_9^195^ VAL_9^255^ VAL_9^259^ GLY_9^197^
BINDING POCKET 2	THR_9^405^ SER_9^406^ ASN_9^552^ THR_9^553^ MET_9^616^ GLY_9^482^ PRO_9^483^ PHE_9^556^ PRO_9^358^ ASN_9^567^ ILE_9^568^ LEU_9^569^ ALA_9^369^ SER_9^370^ THR_9^570^ ALA_9^359^ PRO_9^371^ ALA_9^372^ ARG_9^373^ VAL_9^386^ PRO_9^275^ ALA_9^276^ LEU_9^302^ LYS_9^587^

	ILE_9^295^ GLU_9^297^ LEU_9^300^ PHE_9^589^ GLU_9^292^ LEU_9^301^ LEU_9^357^ GLN_9^274^ GLU_9^547^ ASP_9^549^ ASP_9^564^ PRO_9^566^ MET_9^575^ GLY_9^548^ GLN_9^558^ SER_9^407^ SER_9^550^ LEU_9^551^ TRP_9^608^ ALA_9^611^ TRP_9^546^ VAL_9^573^ GLN_9^602^ SER_9^612^ HIS_9^545^ SER_9^572^ ILE_9^9^ TYR_9^10^ HIS_9^436^ VAL_9^431^ THR_9^433^THR_9^432^ PHE_9^435^ ASP_9^341^ ALA_9^343^ PRO_9^434^ LYS_9^471^ HIS_9^472^ ALA_9^473^ HIS_9^409^ SER_9^342^ VAL_9^345^ GLU_9^350^ ASP_9^13^ GLU_9^14^ GLU_9^17^ ASN_9^411^ ASN_9^404^ GLU_9^410^ THR_9^607^ ASP_9^243^ PRO_9^344^ ASN_9^408^ SER_9^11^ SER_9^12^ SER_9^8^ THR_9^430^ HIS_9^339^ GLY_9^340^ THR_9^466^ HIS_9^335^ THR_9^336^ ARG_9^337^ SER_9^346^ LYS_9^428^ HIS_9^427^ LEU_9^429^ ASP_9^334^ GLY_9^426^ THR_9^331^ SER_9^412^ SER_9^606^ ILE_9^332^ ALA_9^333^ ILE_9^425^ CYS_9^604^ SER_9^605^ ASP_9^413^ LEU_9^414^ THR_9^422^ PRO_9^417^ GLY_9^349^ HIS_9^351^ PRO_9^488^ VAL_9^562^ ALA_9^563^ HIS_9^352^ ALA_9^565^ PRO_9^577^ ALA_9^576^ GLU_9^582^ VAL_9^193^ LEU_9^487^ THR_9^490^ PRO_9^355^ GLY_9^362^ SER_9^363^ GLN_9^489^ PRO_9^491^ SER_9^353^ THR_9^354^ LEU_9^364^ MET_9^486^ LEU_9^348^ LEU_9^484^ PRO_9^361^ SER_9^356^ LEU_9^494^ SER_9^571^ LEU_9^586^ SER_9^579^ ASP_9^583^ VAL_9^270^ MET_9^21^ ALA_9^578^ PRO_9^365^ SER_9^368^ PRO_9^238^ ASN_9^241^ MET_9^1^ LYS_9^92^ LEU_9^555^ LEU_9^574^ PRO_9^603^ CYS_9^347^ SER_9^401^ PRO_9^467^ GLU_9^618^ GLU_9^617^ ARG_9^457^ VAL_9^501^ PHE_9^540^ SER_9^560^ THR_9^559^ GLU_9^366^ LEU_9^498^ PRO_9^561^ ASP_9^497^ HIS_9^493^ VAL_9^495^ ASP_9^16^ LYS_9^32^ ILE_9^91^ GLN_9^237^ GLY_9^93^ PRO_9^94^ ARG_9^437^ ASP_9^438^
BINDING POCKET 3	PRO_9^233^ ASP_9^48^ ARG_9^45^ ASN_9^217^ SER_9^218^ TYR_9^10^ SER_9^11^ ASP_9^243^ TYR_9^244^ VAL_9^345^ CYS_9^347^ MET_9^1^ ASP_9^16^ ASN_9^242^ PHE_9^19^ LYS_9^32^ ALA_9^2^ ARG_9^42^ PRO_9^31^ SER_9^245^ LEU_9^348^ ASN_9^254^ GLN_9^253^ TYR_9^246^ PHE_9^214^ SER_9^33^ LYS_9^35^ GLY_9^34^ ARG_9^3^ LYS_9^216^ TRP_9^43^ LYS_9^84^ GLN_9^215^ LEU_9^232^ ARG_9^81^ VAL_9^240^ THR_9^44^ THR_9^239^ VAL_9^85^ LEU_9^38^ ARG_9^4^ SER_9^257^ VAL_9^259^ ARG_9^36^ HIS_9^258^ PRO_9^260^ GLN_9^77^ ARG_9^73^ ALA_9^234^ GLU_9^251^ALA_9^252^ LYS_9^40^ THR_9^41^ GLN_9^231^ HIS_9^80^ GLU_9^46^ TYR_9^247^ ALA_9^230^ THR_9^212^ PRO_9^228^ GLU_9^132^ ASN_9^179^ ARG_9^165^ LEU_9^220^ MET_9^221^ VAL_9^76^ THR_9^235^ GLY_9^236^ ARG_9^131^ ASP_9^178^ HIS_9^219^ ASN_9^136^ ALA_9^167^ HIS_9^135^ ARG_9^133^ GLN_9^237^ HIS_9^248^ GLU_9^478^ GLN_9^129^ ALA_9^170^ LYS_9^171^ ILE_9^249^ ILE_9^479^ THR_9^177^ GLU_9^168^ ARG_9^176^ TRP_9^134^ ASN_9^139^ LEU_9^138^ VAL_9^142^ PRO_9^112^ GLU_9^141^ PRO_9^174^ GLY_9^175^ LEU_9^173^ LYS_9^113^ SER_9^12^ SER_9^346^ MET_9^486^ LEU_9^484^ PRO_9^5^ SER_9^256^ LEU_9^30^ LYS_9^52^ GLU_9^49^ LEU_9^51^ HIS_9^37^ PRO_9^227^ GLY_9^39^
BINDING POCKET 4	ARG_9^465^ ALA_9^476^ SER_9^509^ GLY_9^510^ GLN_9^554^ SER_9^506^ THR_9^557^ ALA_9^473^ ALA_9^475^ GLU_9^514^ LEU_9^555^ ILE_9^479^ PHE_9^556^ GLY_9^482^ HIS_9^472^ LEU_9^474^ LYS_9^442^ ILE_9^502^ PRO_9^483^ LYS_9^480^ TYR_9^481^ LYS_9^503^ GLN_9^499^ ASN_9^183^ SER_9^187^ ASP_9^507^ HIS_9^248^ ALA_9^180^ ARG_9^190^ LYS_9^485^ HIS_9^184^ SER_9^250^ ILE_9^249^ SER_9^146^ LYS_9^144^ THR_9^145^ LYS_9^143^ TRP_9^147^ ARG_9^176^ ASN_9^186^ GLN_9^253^ THR_9^177^ TYR_9^247^ HIS_9^137^ VAL_9^142^ GLN_9^477^ ASN_9^136^ GLU_9^151^ LYS_9^445^ LYS_9^182^ GLU_9^251^ ALA_9^252^ ILE_9^511^ ALA_9^211^ VAL_9^255^ VAL_9^210^ TRP_9^95^ THR_9^212^ ARG_9^165^ THR_9^440^ VAL_9^441^ ALA_9^230^ ASN_9^179^ LYS_9^97^ ASP_9^100^ GLN_9^444^ THR_9^229^ ASP_9^178^ GLN_9^225^ THR_9^96^ THR_9^443^ PRO_9^140^ GLN_9^101^ TRP_9^166^ ILE_9^104^
BINDING POCKET 5	PRO_9^464^ SER_9^463^ PRO_9^467^ GLU_9^618^ ILE_9^399^ ALA_9^393^ GLU_9^394^ THR_9^534^ GLU_9^531^ LEU_9^396^ THR_9^395^ SER_9^532^ PRO_9^533^ LEU_9^460^ PHE_9^392^ VAL_9^530^ GLN_9^528^ LEU_9^522^ ASN_9^518^ ILE_9^459^ GLY_9^519^ SER_9^462^ GLN_9^397^ PHE_9^398^ PRO_9^521^ PRO_9^520^ THR_9^468^ LYS_9^387^ PHE_9^541^ HIS_9^545^ GLY_9^614^ GLN_9^619^ MET_9^616^ LEU_9^551^ GLN_9^516^ CYS_9^613^ ASN_9^552^ SER_9^612^ GLU_9^461^ SER_9^537^ GLU_9^391^ SER_9^458^ ILE_9^455^ LEU_9^523^ GLU_9^517^ GLY_9^538^ HIS_9^544^ PHE_9^540^ VAL_9^512^ GLY_9^548^ ALA_9^513^ SER_9^550^ THR_9^553^ PHE_9^515^ GLU_9^505^ GLN_9^554^ SER_9^509^ GLU_9^547^ GLN_9^558^ ARG_9^457^

	THR_9^466^ GLU_9^508^ ASP_9^549^ THR_9^557^ PHE_9^556^

Table S14: Active binding site residues of pcna

BINDING POCKET 1	VAL_A^123^ GLN_A^125^ GLN_A^38^ GLU_A^124^ ASP_A^29^ CYS_A^27^ TRP_A^28^ ASN_A^36^ LEU_A^37^ SER_A^39^ MET_A^40^ LEU_A^126^ LEU_A^47^ ALA_A^67^ ASP_A^122^ HIS_A^44^ ALA_A^26^ LEU_A^121^ GLU_A^25^ ASP_A^41^ ILE_A^23^ ASN_A^24^ SER_A^42^ GLN_A^49^ LEU_A^50^ THR_A^51^ HIS_A^246^ GLY_A^127^ LEU_A^66^ MET_A^68^ LEU_A^22^
BINDING POCKET 2	GLN_A^38^ LEU_A^47^ GLN_A^49^ ILE_A^128^ LYS_A^248^ TYR_A^250^ GLU_A^132^ GLU_A^198^ TYR_A^133^ VAL_A^136^ ASN_A^200^ GLN_A^131^ SER_A^228^ MET_A^199^ SER_A^134^ PRO_A^129^ GLU_A^130^ VAL_A^236^ GLU_A^238^ LYS_A^240^ THR_A^226^ HIS_A^246^
BINDING POCKET 3	LEU_A^6^ GLY_A^56^ ILE_A^11^ ALA_A^242^ ASP_A^243^ MET_A^244^ ILE_A^241^ GLN_A^8^ LEU_A^221^ LYS_A^240^ SER_A^222^ PRO_A^220^ LYS_A^14^ SER_A^10^
BINDING POCKET 4	GLY_A^155^ ASP_A^156^ ALA_A^157^
BINDING POCKET 5	SER_A^10^ LYS_A^13^ LYS_A^14^ ASN_A^84^

Table S15: Active binding site residues of top3a

BINDING POCKET 1	LYS_A^409^ SER_A^410^ GLU_A^366^ ASP_A^411^ GLN_A^412^ LYS_A^593^ GLU_A^528^ ASP_A^328^ ASN_A^368^ VAL_A^330^ ASP_A^597^ THR_A^329^ THR_A^365^ ALA_A^413^ THR_A^534^ LYS_A^529^ GLY_A^531^ HIS_A^538^ CYS_A^596^ ILE_A^532^ ASP_A^535^ GLU_A^589^ ALA_A^590^ ARG_A^151^ ARG_A^177^ HIS_A^414^ ALA_A^536^ ARG_A^364^ ASP_A^197^ ALA_A^586^ VAL_A^200^ CYS_A^149^ ILE_A^595^ ASP_A^150^ LEU_A^592^ GLU_A^154^ TYR_A^362^ ARG_A^175^ THR_A^537^ ARG_A^585^ GLU_A^152^ ARG_A^207^ GLU_A^333^ MET_A^348^ ALA_A^539^ GLU_A^540^ LEU_A^588^ HIS_A^541^ VAL_A^204^ ALA_A^203^ LYS_A^345^ CYS_A^244^ GLU_A^352^ GLU_A^41^ ASP_A^148^ ARG_A^349^ ASP_A^211^ GLU_A^346^ ILE_A^156^ GLU_A^543^ HIS_A^92^ GLY_A^91^ THR_A^367^ ILE_A^369^ PHE_A^370^ PRO_A^371^ PRO_A^415^ ARG_A^372^ SER_A^179^ LEU_A^374^ ASP_A^373^ GLU_A^180^ PHE_A^178^ ALA_A^185^ HIS_A^184^ ASN_A^375^ THR_A^188^ THR_A^182^ LEU_A^379^ HIS_A^418^ ALA_A^189^ THR_A^420^ GLN_A^382^ ASN_A^192^ VAL_A^378^ GLU_A^195^ ASN_A^408^ HIS_A^530^
BINDING POCKET 2	SER_A^179^ PRO_A^371^ ARG_A^372^ GLN_A^412^ ILE_A^369^ SER_A^410^ PHE_A^370^ ASP_A^373^ LEU_A^374^ ASN_A^375^ LEU_A^376^ THR_A^377^ PRO_A^404^ PRO_A^402^ ASN_A^406^ HIS_A^184^ ALA_A^185^ THR_A^188^ PRO_A^183^ THR_A^182^ GLN_A^382^ GLU_A^180^ THR_A^420^ LEU_A^379^ THR_A^367^ HIS_A^414^ PRO_A^415^ ALA_A^413^ ASP_A^411^ VAL_A^378^ HIS_A^418^ PRO_A^419^ LYS_A^421^ ASN_A^192^ ARG_A^177^ PHE_A^178^ ALA_A^189^ CYS_A^149^
BINDING POCKET 3	ASP_A^150^ ARG_A^364^ ASP_A^535^ ALA_A^536^ ARG_A^151^ GLU_A^152^ THR_A^537^ GLU_A^540^ TYR_A^362^ GLU_A^352^ ARG_A^207^ GLU_A^41^ ASP_A^148^ ILE_A^156^ HIS_A^92^ THR_A^534^ HIS_A^541^ ASP_A^211^ ARG_A^585^ ALA_A^539^ GLU_A^333^ MET_A^348^ GLY_A^91^ LYS_A^345^ GLU_A^589^ LEU_A^592^ ALA_A^203^ VAL_A^204^ ARG_A^349^ LYS_A^42^ HIS_A^96^ GLN_A^208^ SER_A^90^ LEU_A^94^ THR_A^544^ GLU_A^346^ LYS_A^353^ GLY_A^242^ SER_A^243^ CYS_A^244^ GLN_A^245^ TYR_A^241^ GLY_A^215^ LEU_A^212^ ALA_A^95^ ILE_A^214^ ARG_A^548^ ALA_A^216^ THR_A^219^ PHE_A^126^ SER_A^240^ LEU_A^238^ PRO_A^123^ TRP_A^105^ ARG_A^220^ ASN_A^125^ ASP_A^97^ PHE_A^98^ TYR_A^121^ GLU_A^543^
BINDING POCKET 4	ASP_A^150^ ARG_A^151^ GLU_A^154^ VAL_A^200^ CYS_A^149^ ARG_A^177^ ALA_A^413^ ASP_A^411^ CYS_A^596^ ASP_A^597^

	LYS_A^593^ ASP_A^197^ ASP_A^535^ ARG_A^364^ HIS_A^414^ THR_A^194^ GLU_A^195^ ARG_A^175^ PRO_A^196^ GLN_A^412^ ASN_A^192^ PHE_A^178^ SER_A^179^ GLN_A^198^ ARG_A^199^
BINDING POCKET 5	ASP_A^211^ SER_A^243^ CYS_A^244^ GLN_A^245^ HIS_A^541^ ARG_A^585^ GLY_A^242^ ARG_A^207^ GLU_A^540^ THR_A^544^ TYR_A^241^ LEU_A^212^ GLY_A^215^ ARG_A^548^ ALA_A^216^ THR_A^219^ SER_A^240^ HIS_A^96^ LEU_A^238^ PHE_A^98^ ARG_A^220^ TRP_A^105^

Table S16: Active binding site residues of p73 using three PDB IDs.

PDB ID: 2WQI	BINDING POCKET 1	LEU_A^357^ GLN_A^358^ VAL_A^359^ LEU_A^368^ PHE_A^365^ ASN_A^364^ MET_A^369^ TYR_A^356^ LEU_A^371^ GLU_A^366^ LYS_A^372^ ILE_A^367^ LEU_A^375^ TYR_A^355^ GLU_A^373^ THR_A^354^ GLU_A^376^ ASP_A^353^ GLU_A^352^ GLU_A^379^
	BINDING POCKET 2	LEU_A^368^ MET_A^369^ LYS_A^372^ LYS_A^370^ GLU_A^373^
	BINDING POCKET 3	GLN_A^358^ VAL_A^359^ ARG_A^360^
	BINDING POCKET 4	MET_A^378^ VAL_A^386^ ARG_A^390^ LEU_A^375^ GLU_A^379^
	BINDING POCKET 5	VAL_A^381^ LEU_A^385^ TYR_A^389^ MET_A^378^ VAL_A^386^ SER_A^388^ GLN_A^392^ ARG_A^390^ LEU_A^375^ SER_A^374^ GLU_A^379^ LEU_A^377^ GLN_A^383^ LEU_A^380^ PRO_A^382^
PDB ID : 2XWC	BINDING POCKET 1	ARG_A^268^ ARG_A^300^ ASP_A^301^ ALA_A^304^ ASP_A^305^ HIS_A^308^ ARG_A^293^ ILE_A^294^ CYS_A^295^ PRO_A^270^ GLU_A^291^ SER_A^260^ PRO_A^298^ ARG_A^269^ SER_A^261^ VAL_A^263^ ILE_A^271^ LEU_A^214^ PHE_A^256^ ILE_A^273^ GLY_A^292^ CYS_A^258^ ASN_A^259^ VAL_A^191^ LYS_A^192^ ARG_A^193^ CYS_A^194^ TYR_A^181^ MET_A^257^ ILE_A^215^ PHE_A^290^ PRO_A^179^ CYS_A^262^ GLY_A^264^ VAL_A^190^ PRO_A^195^ ASP_A^189^
	BINDING POCKET 2	ILE_A^273^ ILE_A^274^ PHE_A^290^
	BINDING POCKET 3	LEU_A^148^ LYS_A^149^ LYS_A^182^ LEU_A^272^ SER_A^289^ PHE_A^290^ GLU_A^291^ ASN_A^118^ THR_A^119^ ASP_A^120^ LYS_A^150^ VAL_A^129^ PHE_A^131^ TYR_A^144^ ARG_A^288^ GLU_A^128^ THR_A^130^
	BINDING POCKET 4	GLY_A^172^ PRO_A^239^ THR_A^173^ LEU_A^222^ VAL_A^238^ GLN_A^224^ ALA_A^174^ TYR_A^240^ SER_A^223^ VAL_A^237^ ARG_A^280^ PRO_A^171^ ILE_A^175^ MET_A^279^ ASP_A^281^ GLY_A^282^ GLU_A^278^ ARG_A^176^ VAL_A^226^ GLN_A^283^
	BINDING POCKET 5	PHE_A^203^ GLU_A^205^ GLN_A^207^ ARG_A^201^ ASP_A^202^ ASN_A^204^ ALA_A^156^ ARG_A^216^ GLU_A^218^ ASN_A^255^ MET_A^257^ ARG_A^193^ ALA_A^209^ PRO_A^210^ ALA_A^211^ SER_A^208^ HIS_A^213^ ILE_A^215^ TYR_A^225^
PDB ID : 1DXS	BINDING POCKET 1	GLU_A^21^ SER_A^25^ TYR_A^22^ GLN_A^26^ ALA_A^44^ LYS_A^46^ LEU_A^45^ ASN_A^18^
	BINDING POCKET 2	LEU_A^7^ VAL_A^8^ GLN_A^29^ GLY_A^27^ LEU_A^28^ SER_A^30^ HIS_A^33^ GLN_A^26^ LEU_A^34^ PHE_A^23^ LEU_A^37^ ILE_A^31^
	BINDING POCKET 3	LEU_A^34^ GLN_A^35^ ASN_A^36^ LEU_A^37^ LEU_A^59^ GLN_A^60^ THR_A^38^ TRP_A^56^ ILE_A^39^ LEU_A^42^ HIS_A^33^ LEU_A^62^ ASP_A^41^
	BINDING POCKET 4	LEU_A^45^
	BINDING POCKET 5	PHE_A^10^ LEU_A^14^

Table S17: Active binding site residues of blm using two PDB IDs

PDB ID: 4O3M	BINDING POCKET 1	LEU_A^716^ HIS_A^798^ MET_A^951^ GLU_A^796^ GLY_A^952^ GLY_A^950^ LEU_A^719^ PRO_A^715^ GLN_A^975^ ILE_A^953^ ARG_A^982^ THR_A^832^ ARG_A^979^ ASP_A^954^ THR_A^691^ ALA_A^831^ THR_A^830^ PHE_A^949^ GLU_A^976^ ILE_A^947^ ARG_A^859^ TYR_A^974^ ALA_A^833^ VAL_A^837^ LYS_A^695^ GLY_A^978^ ASP_A^795^ GLU_A^971^ GLN_A^723^ GLY_A^692^ SER_A^696^ GLY_A^972^ ASN_A^834^ PHE_A^1045^ ALA_A^797^ TYR_A^811^ LYS_A^726^ GLY_A^693^ GLY_A^694^ PRO_A^956^ GLN_A^700^ ASP_A^983^ LEU_A^697^ ARG_A^669^ ASP_A^722^ LYS_A^955^ PHE_A^1238^ ASN_A^1239^ GLN_A^672^ ASN_A^1242^ LEU_A^665^ LEU_A^730^ VAL_A^1244^ PHE_A^663^ GLY_A^984^ LYS_A^1270^ GLY_A^1265^ ASN_A^667^ ASP_A^1264^ PHE_A^1241^ THR_A^1245^ SER_A^729^ LYS_A^1248^ ASN_A^861^ GLY_A^981^ PRO_A^690^ HIS_A^860^ MET_A^855^ LEU_A^862^ ASN_A^858^ THR_A^670^ ALA_A^980^ SER_A^856^ PHE_A^857^ SER_A^969^ ILE_A^841^ ARG_A^808^ GLN_A^809^ ASP_A^810^ ARG_A^813^ PRO_A^767^ THR_A^1015^ ARG_A^1016^ THR_A^1018^ HIS_A^1019^ HIS_A^1014^ GLU_A^1017^ ALA_A^948^ GLN_A^844^ LYS_A^968^ ASN_A^1022^ ASP_A^840^ THR_A^946^ TYR_A^894^ PRO_A^967^ LEU_A^966^ ARG_A^836^ TYR_A^1044^ SER_A^718^ LEU_A^829^ LEU_A^727^ THR_A^728^ THR_A^1243^ MET_A^689^ GLY_A^664^ PHE_A^659^ PHE_A^668^ GLU_A^985^ HIS_A^666^
	BINDING POCKET 2	LYS_A^1207^ ASP_A^938^ TRP_A^881^ ASN_A^1194^ ASP_A^1064^ SER_A^1062^ CYS_A^1063^ GLU_A^1193^ LEU_A^867^ LYS_A^1068^ GLU_A^1213^ MET_A^1214^ VAL_A^1215^ LYS_A^1217^ LYS_A^1216^ TYR_A^888^ LEU_A^1219^ GLY_A^1220^ THR_A^1223^ ASP_A^889^ SER_A^890^ GLN_A^937^ THR_A^1243^ ASP_A^957^ GLU_A^1224^ LYS_A^1227^ ARG_A^959^ LYS_A^1247^ GLU_A^1212^ GLU_A^1251^ GLU_A^985^ HIS_A^886^ ILE_A^986^ TYR_A^1237^ VAL_A^1244^ HIS_A^885^ PRO_A^887^ HIS_A^988^ GLN_A^941^ GLN_A^1210^ ARG_A^1211^ ASP_A^1060^ CYS_A^940^ LYS_A^863^ SER_A^1209^ ALA_A^914^ GLY_A^939^ TYR_A^865^ VAL_A^1208^ PRO_A^1059^ CYS_A^1067^ CYS_A^1066^ CYS_A^1055^
	BINDING POCKET 3	GLN_A^975^ GLU_A^976^ GLY_A^978^ ARG_A^979^
	BINDING POCKET 4	ARG_A^669^ VAL_A^1244^ ASP_A^1264^ LEU_A^665^ ASP_A^983^ ASN_A^1242^ ARG_A^982^ GLY_A^984^ LYS_A^726^ PRO_A^956^ THR_A^1245^ THR_A^1243^ GLY_A^1265^ PHE_A^663^ LEU_A^730^ LYS_A^1270^ GLY_A^664^ VAL_A^1266^ THR_A^1267^ PHE_A^1241^ ASP_A^957^ PHE_A^1238^ TYR_A^1237^ SER_A^696^ GLN_A^723^ ASP_A^954^ LEU_A^719^ ASP_A^722^ ASN_A^1239^ SER_A^718^ GLN_A^672^ GLY_A^694^ LYS_A^695^ LEU_A^697^ GLN_A^700^ SER_A^729^ GLY_A^693^ ASN_A^667^ PHE_A^659^ PHE_A^668^ HIS_A^666^ GLY_A^692^ LYS_A^955^ THR_A^691^ ALA_A^831^ GLU_A^796^ ASP_A^795^
	BINDING POCKET 5	ILE_A^1033^ ARG_A^1037^ LEU_A^990^ HIS_A^885^ ASN_A^1032^ ILE_A^986^ LYS_A^1217^ ASP_A^1064^ TYR_A^865^ HIS_A^988^ LEU_A^1004^ MET_A^1007^ GLU_A^1008^ ARG_A^898^ ALA_A^920^ GLY_A^921^ THR_A^946^ SER_A^897^ ILE_A^1005^ LYS_A^968^ ALA_A^948^ ASN_A^1164^ ASP_A^1165^ GLN_A^1166^ ARG_A^1003^ ARG_A^899^ LEU_A^896^ ILE_A^947^ HIS_A^919^ ALA_A^1167^ ARG_A^1000^ GLU_A^900^ LEU_A^1001^ CYS_A^895^ TYR_A^894^ HIS_A^996^

		ASN_A^1162^ ILE_A^1168^ THR_A^999^ THR_A^903^ ALA_A^1169^ LYS_A^872^ GLU_A^976^ THR_A^1110^ PRO_A^871^ ASP_A^997^ MET_A^904^ LEU_A^966^ PRO_A^967^ LYS_A^869^ ALA_A^875^ THR_A^907^ VAL_A^874^ ALA_A^964^ SER_A^965^ MET_A^1113^ ASN_A^1112^ MET_A^1111^ GLU_A^1157^ LYS_A^873^ PHE_A^876^ VAL_A^1171^ TYR_A^995^ LYS_A^870^ THR_A^994^ LYS_A^1147^ TYR_A^888^ GLN_A^937^ CYS_A^940^ GLN_A^941^ SER_A^890^ ASP_A^889^ LYS_A^1227^ GLU_A^1143^ GLU_A^1224^ THR_A^1223^ PRO_A^887^ GLY_A^1220^ TYR_A^993^ ASP_A^957^ TYR_A^1237^ PRO_A^868^ ARG_A^959^ THR_A^1243^ GLU_A^1031^ GLU_A^1221^ LEU_A^867^ ASP_A^877^ PHE_A^992^ CYS_A^1030^ LEU_A^1246^ HIS_A^1140^ ARG_A^1144^ GLU_A^880^ VAL_A^866^ TRP_A^881^ LEU_A^1219^ LYS_A^884^ HIS_A^886^ LYS_A^1216^ SER_A^987^ GLU_A^985^ LYS_A^1247^ THR_A^1192^ ASN_A^1065^ ARG_A^883^ LYS_A^1068^ LYS_A^863^ GLU_A^1213^ MET_A^1190^ ASN_A^1194^ GLY_A^984^ GLU_A^1191^ VAL_A^1215^ GLU_A^1193^ ASP_A^1060^ GLU_A^1212^ GLU_A^1251^ LYS_A^1207^ GLN_A^1210^ CYS_A^1063^ SER_A^1209^ SER_A^1062^ TYR_A^864^ VAL_A^1208^ PRO_A^1059^ ARG_A^1211^ VAL_A^1061^ CYS_A^1067^ CYS_A^1066^ CYS_A^1055^ LYS_A^1056^
PDB ID: 5LUP	BINDING POCKET 1	ILE_C^373^ HIS_C^374^ MET_C^376^ GLU_C^377^ HIS_C^378^ CYS_C^380^ ARG_C^407^ LEU_C^411^ ILE_C^379^ ILE_C^383^ LEU_C^400^ LEU_C^410^ ASP_C^384^ GLN_C^403^ ARG_C^404^ ILE_C^406^
	BINDING POCKET 2	LYS_C^381^ ASP_C^384^ LEU_C^411^ ARG_C^404^ ARG_C^408^
	BINDING POCKET 3	LEU_C^368^ GLN_C^369^ LEU_C^372^
	BINDING POCKET 4	GLU_C^377^ ARG_C^407^ LEU_C^411^ GLN_C^403^ ILE_C^406^ LEU_C^410^
	BINDING POCKET 5	ASP_C^384^ ARG_C^408^ LEU_C^411^

Domain Analysis of target proteins under study using MOTIF Search and ScanProsite

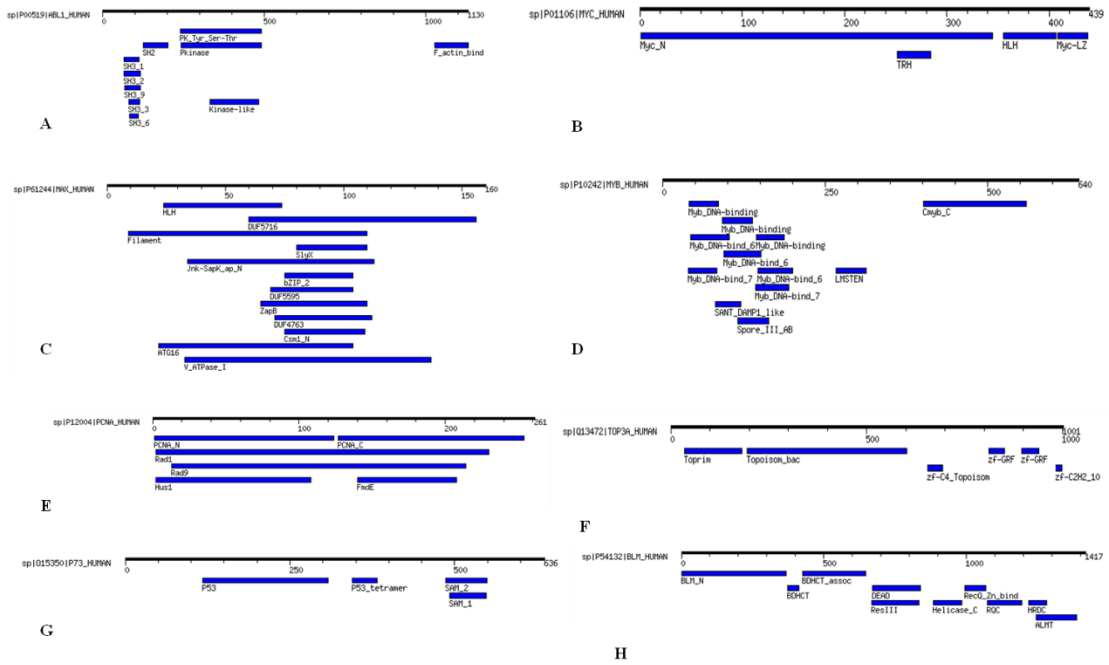

Figure 2: Graphical representation of domains of proteins- (A) abl1, (B) myc, (C) max, (D) myb, (E) pcna, (F) top3a, (G) p73, (H) blm. The output from both the tools used, gave a very similar domain analysis for a given protein.

Table S18: Domain analysis for ALL protein

abl1

DOMAIN ID	POSITION	DESCRIPTION
PK_Tyr_Ser-Thr	242..492	Protein tyrosine and serine/threonine kinase
Pkinase	244..491	Protein kinase domain
F_actin_bind	1026..1130	F-actin binding
SH2	127..202	SH2 domain
SH3_1	67..113	SH3 domain
SH3_2	66..118	Variant SH3 domain
SH3_9	68..117	Variant SH3 domain
SH3_3	82..116	Bacterial SH3 domain
Kinase-like	333..483	Kinase-like
SH3_6	83..112	SH3 domain (SH3b1 type)

myc

DOMAIN ID	POSITION	DESCRIPTION
Myc_N	1..345	Myc amino-terminal region
Myc-LZ	408..438	Myc leucine zipper domain
HLH	355..407	Helix-loop-helix DNA-binding domain
TRH	252..284	Thyrotropin-releasing hormone (TRH)

max

DOMAIN ID	POSITION	DESCRIPTION
HLH	24..74	Helix-loop-helix DNA-binding domain
DUF5716	60..156	Family of unknown function (DUF5716)
Filament	9..110	Intermediate filament protein
SlyX	80..110	SlyX
Jnk-SapK_ap_N	34..113	JNK_SAPK-associated protein-1
bZIP_2	75..104	Basic region leucine zipper

DUF5595	69..104	Domain of unknown function (DUF5595)
ZapB	65..110	Cell division protein ZapB
DUF4763	71..112	Domain of unknown function (DUF4763)
Csm1_N	75..109	Csm1 N-terminal domain
ATG16	22..104	Autophagy protein 16 (ATG16)
V_ATPase_I	33..137	V-type ATPase 116kDa subunit family

myb

DOMAIN ID	POSITION	DESCRIPTION
Cmyb_C	401..560	C-myb, C-terminal
Myb_DNA-binding	41..86,92..138,145..187	Myb-like DNA-binding domain
Myb_DNA-bind_6	43..103,95..152,147..201	Myb-like DNA-binding domain
LMSTEN	267..313	LMSTEN motif
Myb_DNA-bind_7	40..84,143..194	Myb DNA-binding like
SANT_DAMP1_like	81..121	SANT/Myb-like domain of DAMP1
Spore_III_AB	116..164	Stage III sporulation protein AB (spore_III_AB)

pcna

DOMAIN ID	POSITION	DESCRIPTION
PCNA_C	127..254	Proliferating cell nuclear antigen, C-terminal domain
PCNA_N	1..124	Proliferating cell nuclear antigen, N-terminal domain
Rad1	2..230	Repair protein Rad1/Rec1/Rad17
Rad9	13..214	Rad9
Hus1	2..108	Hus1-like protein
FmdE	140..208	FmdE, Molybdenum formylmethanofuran dehydrogenase operon

top3a

DOMAIN ID	POSITION	DESCRIPTION
Topoisom_bac	196..603	DNA topoisomerase
zf-GRF	811..851,896..939	GRF zinc finger
Toprim	36..181	Toprim domain
zf-C4_Topoisom	656..693	Topoisomerase DNA binding C4 zinc finger
zf-C2H2_10	983..998	C2H2 zinc-finger

p73

DOMAIN ID	POSITION	DESCRIPTION
P53	118..308	P53 DNA-binding domain
P53_tetramer	345..383	P53 tetramerisation motif
SAM_2	486..549	SAM domain (Sterile alpha motif)
SAM_1	492..548	SAM domain (Sterile alpha motif)

blm

DOMAIN ID	POSITION	DESCRIPTION
BLM_N	1..367	N-terminal region of Bloom syndrome protein
BDHCT_assoc	425..647	BDHCT-box associated domain on Bloom syndrome protein
BDHCT	372..411	BDHCT (NUC031) domain
DEAD	671..838	DEAD/DEAH box helicase
RecQ_Zn_bind	995..1067	RecQ zinc-binding
RQC	1072..1195	RQC domain
Helicase_C	883..983	Helicase conserved C-terminal domain
HRDC	1217..1281	HRDC domain
ResIII	667..833	Type III restriction enzyme, res subunit
ALMT	1245..1388	Aluminium activated malate transporter

Distribution of Binding Affinity of Compound 88 with eight target proteins as predicted via AutoDock Vina based Virtual Screening

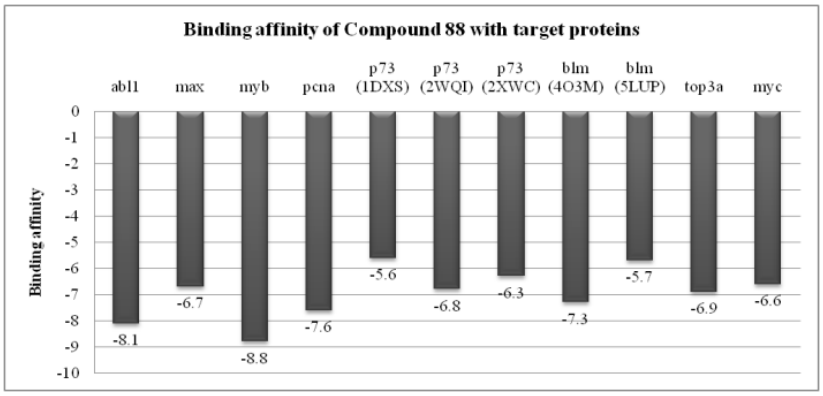

Figure 3: Distribution of binding affinity of Compound 88 with target proteins as predicted by AutoDock Vina; X-axis corresponds to target proteins; Y-axis corresponds to binding affinity

3D Ligand Similarity Search (LS-align) - Compound 3 and ATRA

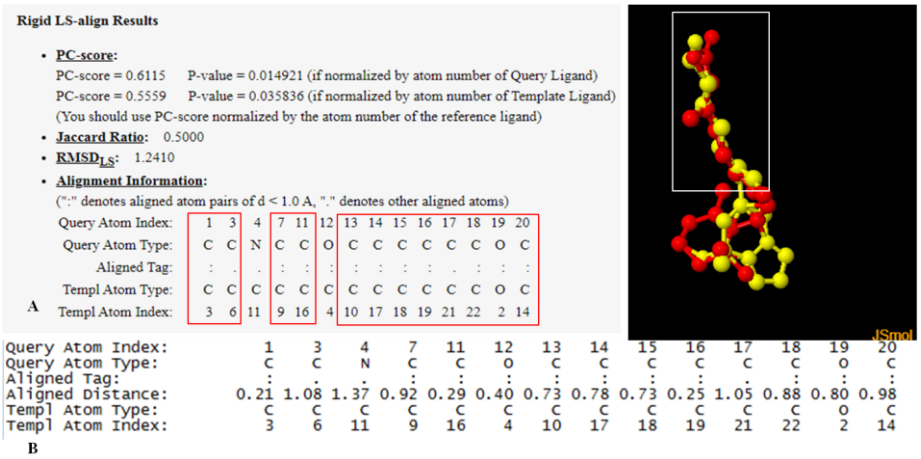

Figure 4: (A) The rigid align scores of query (Compound 3-yellow) and template (ATRA-red) ligands; the red box indicates toward strongly aligned atom pairs of the aligned distance <1Å; Query ligand is depicted in yellow and template ligand is depicted in red; the white box depicting the aligned region between compound 3 and ATRA; (B) The rigid align distance (Å) between query (Compound 3) and template (ATRA) ligand atom pairs. Compound 3 and ATRA were found to share approximately 85% atomic identity

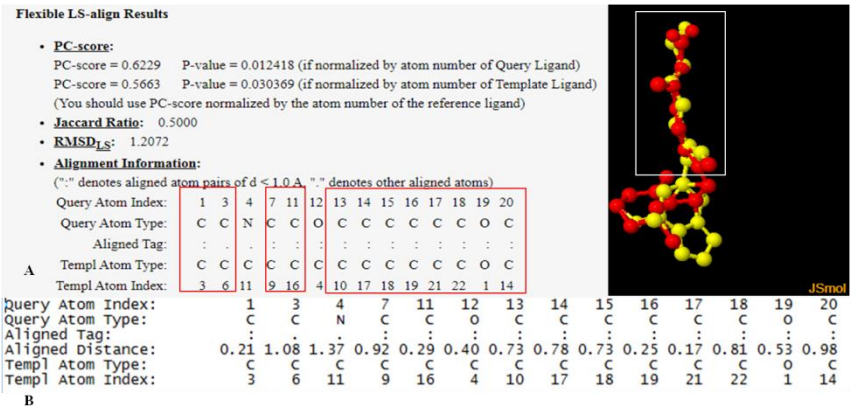

Figure 5: (A) The flexible align scores of query (Compound 3-yellow) and template (ATRA-red) ligands; the red box indicates toward strongly aligned atom pairs of the aligned distance <1Å; Query ligand is depicted in yellow and template ligand is depicted in red; the white box depicting the aligned region between compound 3 and ATRA; (B) The flexible align distance (Å) between query (Compound 3) and template (ATRA) ligand atom pairs. Compound 3 and ATRA were found to share approximately 85% atomic identity

Molecular Docking of ATRA with myc and p73

ATRA was docked with proteins myc and p73. We observed that the atoms of ATRA and Compound 3 involved in interactions with target proteins were similar (**Fig.3**).

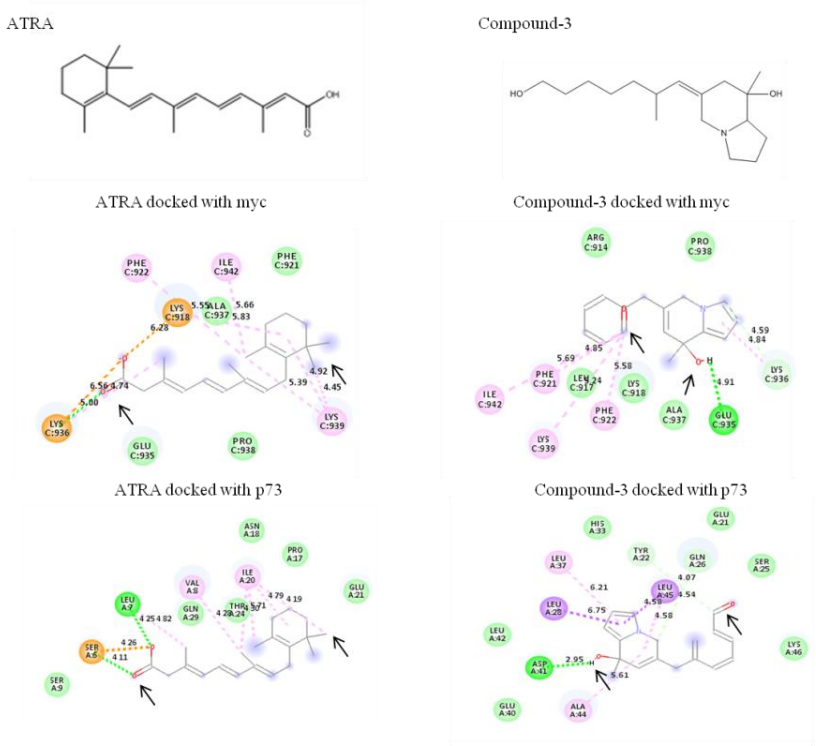

Figure 6: Structure of ATRA and Compound 3 and their docking with proteins myc and p73 respectively; the arrows indicate atoms involved in protein binding. The atoms of both the ligands had similar binding atoms with the respective protein, confirming similarity index between the two biomolecules

Distribution of Binding Energy of UBS109 with eight target proteins as predicted via AutoDock Tools

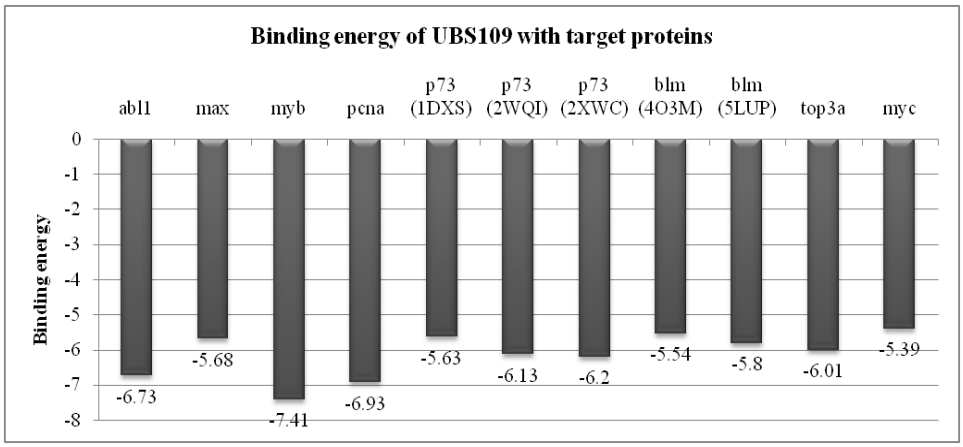

Figure 7: Distribution of binding energy of UBS109 with target proteins as predicted by AutoDock Tools; X-axis corresponds to target proteins; Y-axis corresponds to binding energy